Spectroscopic Study of the Fermi Level Electronic Structure of Single-Walled Carbon Nanotubes

ARTICLE *in* NANO LETTERS · DECEMBER 2001

Impact Factor: 13.59 · DOI: 10.1021/nl0156639

NANO LETTERS

2002
Vol. 2, No. 2
155−159

Spectroscopic Study of the Fermi Level Electronic Structure of Single-Walled Carbon Nanotubes

M. E. Itkis, S. Niyogi, M. E. Meng, M. A. Hamon, H. Hu, and R. C. Haddon*

Center for Nanoscale Science and Engineering, Departments of Chemistry and Chemical & Environmental Engineering, University of California, Riverside, California 92521-0403

Received November 13, 2001; Revised Manuscript Received December 7, 2001

ABSTRACT

The electronic structure of single-walled carbon nanotubes (SWNTs) is investigated by transmission spectroscopy of thin films. Hole-doping of SWNTs, as a result of purification, leads to free carrier absorption in the far-IR spectral range. Thermal cycling de-dopes SWNTs, transferring spectral weight from the far-IR to the interband transitions in the near-IR spectral range. After the nanotubes are de-doped, a diameter dependent peak in the far-IR is apparent at ~100 cm^{-1}, which we ascribe to a curvature induced energy gap in the DOS of nonarmchair metallic SWNTs.

From the time of their discovery in 1993,[1] it has been recognized that single walled carbon nanotubes (SWNTs) possess a unique electronic structure (Figure 1). Depending on helicity and diameter, these 1-D nanostructures may be metals or semiconductors.[2−5] The electronic structure of the SWNTs is related to a 2-D graphene sheet, but because of the radial confinement of the wave function the continuous electronic density of states (DOS) in graphite divides into a series of spikes in SWNTs that are referred to as Van Hove singularities. Electronic transitions between these singularities give rise to prominent features in scanning tunneling spectroscopy (STS)[6,7] and optical spectroscopy.[8−11]

However, the principal point of interest is the electronic structure of the SWNTs at the Fermi level. This region of the electronic spectrum is difficult to investigate experimentally but is vital in any discussion of the metallic character of the SWNTs and particularly in addressing questions related to extrinsic effects such as nanotube doping by the environment and intrinsic features such as the presence of energy gaps induced by curvature or bundling. It was theoretically predicted that the finite and monotonic DOS in metallic SWNTs would be distorted near the Fermi level by the formation of a small energy gap due to the finite curvature of the graphene sheet that exists in nanotubes[12,13] or by pseudogap formation due to intertube interaction (Figure 1).[14−17]

Far-IR reflectance measurements on optically thick films of laser-vaporization grown SWNTs (diameter 1.2 nm) revealed a Lorentzian-like feature at 17 meV.[18] The authors suggested that this far-IR absorption band is due to the curvature induced gap in metallic SWNTs.[12,13] Far-IR absorptions could also arise from extrinsic effects, such as impurities and defect induced states within the band gap of

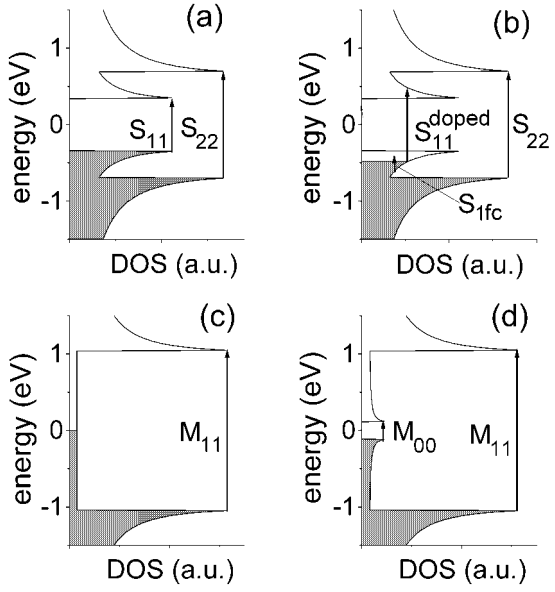

Figure 1. Schematic representation of the density of states (DOS) of SWNTs contributing to the near-IR and far-IR absorption. (a) Semiconducting SWNT; S_{11} and S_{22} correspond to the first and second interband transitions in the near-IR spectral range. (b) Hole-doped semiconducting SWNT; first interband transition (S_{11}^{doped}) is shifted to higher energy due to depletion of the conduction band; intraband transitions involving free carriers (S_{1fc}) contribute to the far-IR absorption. (c) Metallic SWNT; M_{11} is the first metallic transition in the near-IR range. (d) Small gap semiconductor derived from metallic SWNT; M_{00} is the far-IR transition across the curvature induced energy gap in zigzag and chiral metallic SWNTs.

10.1021/nl0156639 CCC: $22.00
Published on Web 12/28/2001

semiconducting SWNTs. Further evidence for the existence of a small energy gap in SWNTs was obtained in an experiment in which an individual SWNT was used as the active semiconductor in a field effect transistor (FET).[19] More recently, an STS study in combination with atomic resolution scanning tunneling microscopy (STM) imaging showed the presence of a small energy gap in metallic zigzag and armchair SWNTs.[20] It was demonstrated that the energy gap varied with the SWNT diameter (d) as $1/d^2$, in excellent agreement with the theoretically predicted behavior of the gap induced by SWNT wall curvature[12,13,21] and intertube interaction.[15−17,22]

In this letter, we probe the density of states (DOS) of SWNTs near the Fermi level as a function of SWNT diameter using far-IR transmission spectroscopy of thin films. We find that the far-IR absorption band shifts to higher energies with decreasing SWNT diameters, in agreement with the behavior expected for a curvature induced energy gap in metallic SWNTs. We also show that the standard methods that are used to remove impurities from the as-prepared SWNT material lead to hole-doped purified SWNTs. This significantly modifies the DOS of the SWNTs, shifting spectral weight from the intrinsic transitions between the first set of singularities in the semiconducting SWNTs to extrinsic absorptions near the Fermi level (Figure 1).

Crude SWNTs contain up to 80 wt % of amorphous carbon, catalyst, and nanoparticles,[23] and these impurities can mask the intrinsic electronic properties of SWNTS. To remove these contaminants, several vigorous purification techniques have evolved that provide materials approaching 90% purity.[23−26] Three types of as-prepared and purified SWNT material were used for this study: (1) electric arc produced material (A-SWNT, CarboLex, Inc), obtained by use of Ni−Y catalyst (SWNT diameters 1.37 ± 0.1 nm[27]); (2) laser vaporization produced material (L-SWNT, Tubes@Rice), obtained by use of Co−Ni catalyst (SWNT diameters of 1.22 ± 0.1 nm[24,28]); (3) material produced by gas-phase catalysis (HiPCO process, H−SWNT, Carbon Nanotechnologies, Inc, SWNT diameters 0.8 ± 0.1 nm[28,29]). Homogeneous SWNT dispersions were obtained by sonication in methanol or *N*,*N*-dimethylformamide in the case of A- and L-SWNTs, and in 1,2-dichlorobenzene in the case of H−SWNTs. Thin films of the SWNTs were prepared by spraying the dispersions on heated (180 °C) optical substrates. By utilizing sapphire, zinc selenide, and silicon substrates we were able to cover the UV to far-IR spectral range (50000−10 cm^{-1}). Film thicknesses ($t = 0.1-0.5\ \mu$m) were limited to the range of optical densities $\alpha t < 1$, (α − absorption coefficient) to minimize light scattering. Ten films of each type of SWNT material were investigated, and the results were found to be reproducible within each group.

Figure 2(a, b, c) shows absorption spectra of purified SWNTs from all three sources in comparison with as-prepared material. The 50000−15000 cm^{-1} spectral range is dominated by the π-plasmon absorption, which shows a maximum at 37 000 cm^{-1} (4.6 eV).[30] No significant difference in this feature between as-prepared and purified SWNTs was observed. Interband transitions between the principal

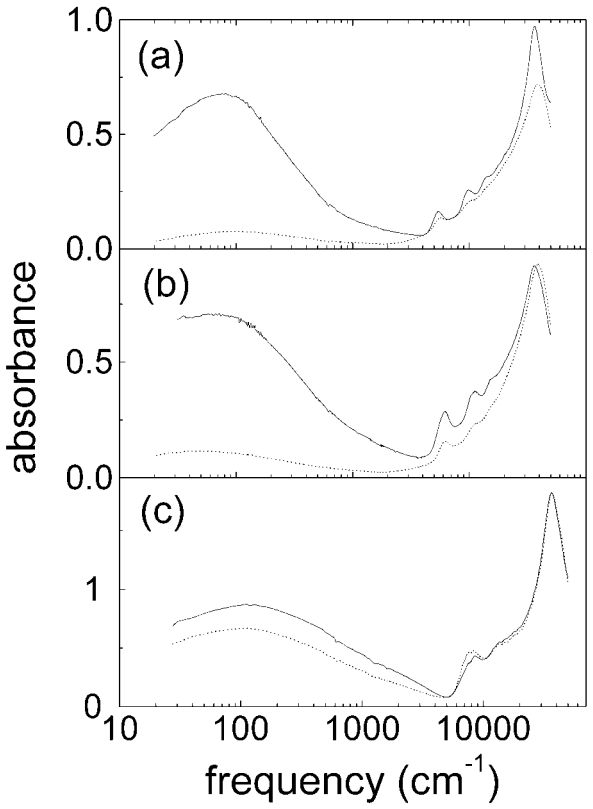

Figure 2. Absorbance spectra of purified (solid line) and as-prepared (dotted line) thin films of the SWNT material produced by (a) electric arc technique (A-SWNTs), (b) laser ablation (L-SWNTs), (c) HiPCO process (H-SWNTs).

mirror spikes in the DOS of semiconducting (Figure 1a, S_{11} and S_{22}) and metallic (Figure 1c, M_{11}) SWNTs appear between 4000 and 15 000cm^{-1}.[8−11] Purification intensifies these intrinsic SWNT spectral features in case of A- and L-SWNT (Figure 2a, b).

The most striking feature in the spectra of purified SWNT films is the intense peak in the far-IR region with an absorption maximum several times higher than that of the interband absorption peaks (S_{11}, S_{22}, and M_{11}) in the near-IR region. For A- and L-SWNT films, the far-IR absorption of as-prepared material is an order of magnitude lower than that of the corresponding purified material. This suggests that a component of the far-IR absorption is due to defects and impurity states introduced during the purification. The effects of environmental dopants on SWNTs have already been reported.[31−33] A high density (2−5 atomic percent) of defective (acidic) carbon sites was detected by titration experiments on purified SWNTs.[34,35] The purified H−SWNT sample shows a much smaller (∼20%) increase in far-IR intensity, and this is probably associated with the milder purification process that has been used on this sample.[36]

Figure 3 shows a comparison between the absorption spectra of purified L-SWNT films before and after heating at 350 °C in a dynamic vacuum (10^{-6} Torr) for 90 min. We observe a strong increase in intensity of the interband absorptions, especially for the first interband transition (S_{11}) of the semiconducting SWNTs, and a significant decrease in the far-IR absorbance together with the formation of a

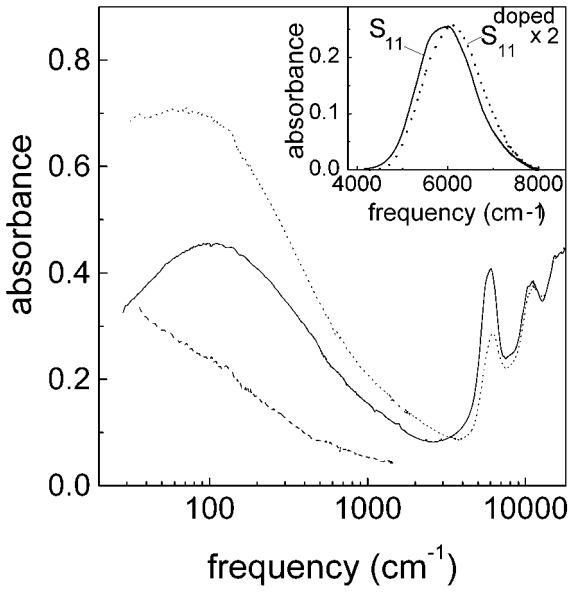

Figure 3. Spectra of a film of purified L-SWNTs before (dotted line) and after (solid line) heating under vacuum at 350 °C and the difference spectra (dashed line) corresponding to the change in absorption due to heat treatment. Inset shows enlarged region of the first semiconducting transition before (S_{11}^{doped}, dotted line, shifted to higher energy) and after (S_{11}, solid line) heat treatment. Both spectra are baseline corrected.

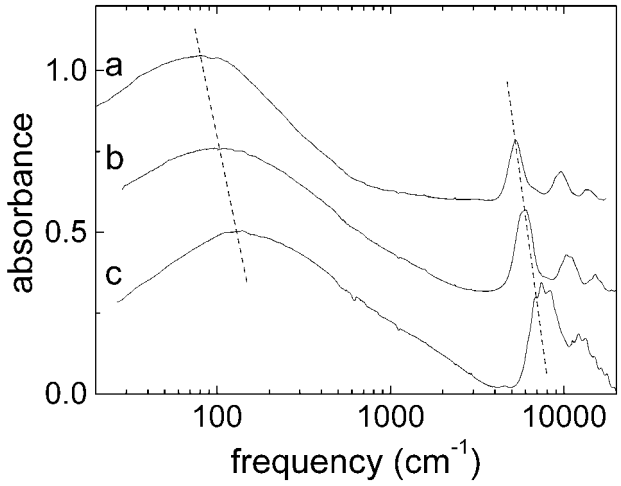

Figure 4. Absorption spectra of the films of the SWNTs produced by electric arc discharge (curve a, SWNTs diameter 1.37 ± 0.1 nm), by laser ablation process (curve b, SWNTs diameter 1.22 ± 0.1 nm), by HiPCO process (curve c, SWNTs diameter 0.80 ± 0.1 nm). Dashed lines delineate the synchronous shift in the near- and far-IR absorption bands with changing SWNT diameter. Spectra have been offset for clarity.

maximum in the spectrum just above100 cm^{-1}. Note the shift to higher energies of the first interband transition for untreated films in comparison with the thermally treated material (inset in Figure 3). Similar results were observed for both A- and H-purified SWNT films (not shown). For the as-prepared SWNT material, no significant changes in absorption spectra were observed on thermal cycling.

The effect of heating on the absorbance of the purified films in the near-IR region is indicative of the modification of the interband transitions, which accompanies doping (de-doping) of SWNT bundles.[10,37,38] Nitric acid used in the purification procedure can partially exfoliate and intercalate SWNT bundles,[39] and the intercalation of nitric acid into graphite is known to be accompanied by hole doping of the graphene sheet.[5,40] It is therefore likely that, after purification, the valence band of the semiconducting SWNTs is partially depleted due to oxidation (Figure 1b) and that the material is left as salts of the form $(SWNT^{n+})(HNO_3)_m(NO_3^-)_n$. This doping effect explains the decrease in intensity and the shift of the optical transition between the first pair of Van-Hove singularities in the DOS to higher energies (Figure 1a, c and 3). The doping will serve to pin the Fermi level in the valence band, and the holes behave as free carriers and produce a strong absorption in the far-IR (transition S_{1fc}, Figure 1). Upon heating, the trapped NO_3^- counterions are removed and the valence band refilled; this serves to restore the strength of the interband transition and eliminates the contribution of doping-induced free carriers to the absorptions in the far-IR range. It also accounts for the shift to lower energy of the S_{11} transition in the de-doped nanotube, because of the refilling of the valence band. Unlike A- and L-SWNTs the intensity of the first semiconducting transition of the as-prepared H-SWNT is higher than that of the purified material (Figure 1c). This is because of the higher purity (97 atomic percent) of as-prepared H-SWNT material[28,29] and the doping introduced by the purification. Also shown in Figure 3 is the spectrum of difference in absorption between heated and unheated SWNT films. This featureless increase in absorption toward low energy is partially due to intraband transition (S_{1fc}, Figure 1) involving free holes introduced into the valence band.

Thus, the doping process introduces extrinsic features into the far-IR region of the electronic spectrum of SWNT films. Below we show that our experiments also provide evidence for intrinsic electronic effects in the SWNTs that are associated with small energy gaps introduced into the continuous DOS at the Fermi level as a result of the finite curvature of the SWNTs.[12,13,15−17] We have argued that the purification process introduces holes into the valence band of the SWNTs that lead to an increase in the far-IR absorption in purified SWNTs. However, Figure 2 shows that the far-IR absorption peak is also present in the as-prepared SWNT material and is an intrinsic feature of SWNTs. Moreover, the ratio of the intensity of the first interband transition (after subtracting the π-plasmon background) to the height of far-IR feature is about 1:1.5, which is very similar to the intensity ratios seen in the purified SWNTs.

Figure 4 shows a comparison between the absorbance spectra of thermally cycled A-, L-, and H-SWNT films after subtracting the smooth background due to the π-plasmon resonance. Both the near-IR and far-IR spectral features show a synchronous shift toward higher energy as the diameter of the SWNT decreases, and this behavior is seen in all of our films. Interband transitions S_{11}, S_{22}, and M_{11}(Figure 1) contribute to the near-IR part of the spectra. The $1/d$ dependence of the separations between mirror peaks in the DOS was predicted within the framework of the tight-binding

model[2,3] and was confirmed experimentally.[6−11] The shift of the far-IR absorption peak to higher energies with decreasing SWNT diameter correlates qualitatively with the predicted diameter dependence of the curvature induced energy gap in metallic SWNTs[12,13] and with the expected effect of intertube interactions on armchair (n,n) nanotubes.[15−17]

For A-, L-, and H-SWNTs, we adopt the following nanotube diameters: $d = 1.37 \pm 0.1$, 1.22 ± 0.1, and 0.8 ± 0.1 nm, respectively, on the basis of transmission electron microscope and X-ray diffraction measurements.[24,27,28] The far-IR absorption maxima (Figure 4) are located at 81 ± 8 cm^{-1} (10.1 ± 1.0 meV) for A-SWNTs, at 107 ± 6 cm^{-1} (13.2 ± 0.7 meV) for L-SWNTs, and at 129 ± 9 cm^{-1} (16.0 ± 1.1 meV) for H-SWNTs, as determined by averaging the results obtained for 10 films of each type of SWNT. These values are significantly lower than the energy gaps obtained by the STM technique[20] but very similar to the values obtained from far-IR reflectance[18] and FET measurements[19] at a given SWNT diameter. According to the calculations,[12,13] the curvature induced energy gap (E_g) in the metallic SWNTs depends on two important parameters: the SWNT diameter (d) and the chiral angle (ϕ) with respect to the (n,n) direction: $E_g = (\gamma a^2/4d^2)\sin 3\phi$, where $\gamma = 2.7$ eV (resonance integral), $a = 0.1424$ nm (C−C bond length).[21]

The STM measurements were carried out on zigzag metallic SWNTs with indices of (9,0), (12,0), (15,0),[20] and are therefore of maximum chiral angle $\phi = 30°$. The far-IR spectroscopic studies employed bulk samples with a statistical distribution of chiralities, so that the measurements do not correspond to the energy gap of a single nanotube type, but rather to a sample average. Using the analytical expression for the effect of curvature on nonarmchair metallic SWNTs,[21] we calculate an energy gap for a (15,0) zigzag SWNT of $E_g = 29.6$ meV ($d = 1.19$ nm, $\phi = 30°$), while a (10,7) chiral SWNT has an energy gap of $E_g = 9.1$ meV ($d = 1.17$ nm, $\phi = 5.8°$). Our experimental values for the energy gaps of the A- and L-SWNTs are close to the median energy gap based on the possible ϕ values. The H-SWNTs show the highest energy gap among all three types of SWNT material investigated, as expected for the SWNTs of smallest diameter and highest curvature.

In summary, we have probed the nature of the electronic structure of the SWNTs in the vicinity of the Fermi level. By correlating this information with the behavior of the conduction and valence bands, we are able to provide a comprehensive picture of the DOS of pristine and doped SWNTs. By measuring the transmittance spectra of SWNT films with different diameter distributions we found that the peak in the far-IR shifts to higher energy synchronously with the near-IR bands as the average SWNT diameter decreases. We assigned the presence of this feature in the far-IR to the curvature induced energy gap in nonarmchair metallic SWNTs. We showed that standard purification methods produce hole-doped SWNTs. Thermal treatment in a vacuum eliminates the effect of doping and shifts the intraband absorption of hole states in the far-IR part of the spectra to the interband transitions between the first set of singularities in the semiconducting SWNTs.

Acknowledgment. The work was supported by the MRSEC Program of the National Science Foundation under Award Number DMR-9809686, and by the Office of Naval Research under Award Number N00014-99-1-0770.

References

(1) Iijima, S.; Ichihashi, T. *Nature (London)* **1993**, *363*, 603−605.
(2) Saito, R.; Fujita, M.; Dresselhaus, G.; Dresselhaus, M. S. *Phys. Rev. B* **1992**, *46*, 1804−1811.
(3) Mintmire, J. W.; Dunlap, B. I.; White, C. T. *Phys. Rev. Lett.* **1992**, *68*, 631−634.
(4) Hamada, N.; Sawada, S.-I.; Oshiyama, A. *Phys. Rev. Lett.* **1992**, *68*, 1579−1581.
(5) Dresselhaus, M. S.; Dresselhaus, G.; Eklund, P. C. *Science of Fullerenes and Carbon Nanotubes*; Academic: San Diego, 1996.
(6) Wildoer, J. W. G.; Venema, L. C.; Rinzler, A. G.; Smalley, R. E.; Dekker, C. *Nature (London)* **1998**, *391*, 59−61.
(7) Odom, T. W.; Huang, J.-L.; Kim, P.; Lieber, C. M. *Nature (London)* **1998**, *391*, 62−64.
(8) Chen, J.; Hamon, M. A.; Hu, H.; Chen, Y.; Rao, A. M.; Eklund, P. C.; Haddon, R. C. *Science* **1998**, *282*, 95−98.
(9) Kataura, H.; Kumazawa, Y.; Maniwa, Y.; Umezu, I.; Suzuki, S.; Ohtsuka, Y.; Achiba, Y. *Synth. Met.* **1999**, *103*, 2555−2558.
(10) Petit, P.; Mathis, C.; Journet, C.; Bernier, P. *Chem. Phys. Lett.* **1999**, *305*, 370−374.
(11) Jost, O.; Gorbunov, A. A.; Pompe, W.; Pichler, T.; Friedlein, R.; Knupfer, M.; Reibold, M.; Bauer, H.-D.; Dunsch, L.; Golden, M. S.; Fink, J. *App. Phys. Lett.* **1999**, *75*, 2217−2219.
(12) Blase, X.; Benedict, L. X.; Shirley, E. L.; Louie, S. G. *Phys. Rev. Lett.* **1994**, *72*, 1878−1881.
(13) Kane, C. L.; Mele, E. J. *Phys. Rev. Lett.* **1997**, *78*, 1932−1935.
(14) Delaney, P.; Choi, J. H.; Ihm, J.; Louie, S. G.; Cohen, M. L. *Nature* **1998**, *391*, 466−468.
(15) Kwon, Y. K.; Saito, S.; Tomanek, D. *Phys. Rev. B* **1998**, *58*, R13314−R13317.
(16) Maarouf, A. A.; Kane, C. L.; Mele, E. J. *Phys. Rev. B* **2000**, *61*, 11156−11165.
(17) Stahl, H.; Appenzeller, J.; Martel, R.; Avouris, P.; Lengeler, B. *Phys. Rev. Lett.* **2000**, *85*, 5186−5189.
(18) Ugawa, A.; Rinzler, A. G.; Tanner, D. B. *Phys. Rev. B* **1999**, *60*, R11305−R11308.
(19) Zhou, C.; Kong, J.; Dai, H. *Phys. Rev. Lett.* **2000**, *84*, 5604−5607.
(20) Ouyang, M.; Huang, J.-L.; Cheung, C. L.; Lieber, C. M. *Science* **2001**, *292*, 702−705.
(21) Kleiner, A.; Eggert, S. *Phys. Rev. B* **2001**, *63*, 073408-1-073408-4.
(22) Rao, A. M.; Chen, J.; Richter, E.; Eklund, P. C.; Haddon, R. C.; Venkateswaran, U. D.; Kwon, Y.-K.; Tomanek, D. *Phys. Rev. Lett.* **2001**, *86*, 3895−3898.
(23) Dillon, A. C.; Gennet, T.; Jones, K. M.; Alleman, J. L.; Parilla, P. A.; Heben, M. J. *Adv. Mater.* **1999**, *11*, 1354−1358.
(24) Rinzler, A. G.; Liu, J.; Dai, H.; Nilolaev, P.; Huffman, C. B.; Rodriguez-Macias, F. J.; Boul, P. J.; Lu, A. H.; Heymann, D.; Colbert, D. T.; Lee, R. S.; Fischer, J. E.; Rao, A. M.; Eklund, P. C.; Smalley, R. E. *Appl. Phys. A* **1998**, *67*, 29−37.
(25) Chiang, I. W.; Brinson, B. E.; Smalley, R. E.; Margrave, J. L.; Hauge, R. H. *J. Phys. Chem. B* **2001**, *105*, 1157−1161.
(26) Liu, J.; Rinzler, A. G.; Dai, H.; Hafner, J. H.; Bradley, R. K.; Boul, P. J.; Lu, A.; Iverson, T.; Shelimov, K.; Huffman, C. B.; Rodriguez-Macias, F.; Shon, Y.-S.; Lee, T. R.; Colbert, D. T.; Smalley, R. E. *Science* **1998**, *280*, 1253−1255.
(27) Ichida, M.; Mizuno, S.; Tani, Y.; Saito, Y.; Nakamura, A. *J. Phys. Soc. Jpn* **1999**, *68*, 3131−3133.
(28) Nikolaev, P.; Bronikowski, M. J.; Bradley, R. K.; Rohmund, F.; Colbert, D. T.; Smith, K. A.; Smalley, R. E. *Chem. Phys. Lett.* **1999**, *313*, 91−97.
(29) Hafner, J. H.; Bronikowski, M. J.; Azamian, B. R.; Nikolaev, P.; Rinzler, A. G.; Colber, D. T.; Smith, K. A.; Smalley, R. E. *Chem. Phys. Lett.* **1998**, *296*, 195−202.
(30) Pichler, T.; Knupfer, M.; Golden, M. S.; Fink, J.; Rinzler, A.; Smalley, R. E. *Phys. Rev. Lett.* **1998**, *80*, 4729−4732.
(31) Collins, P. G.; Bradley, K.; Ishigami, M.; Zettl, A. *Science* **2000**, *287*, 1801.
(32) Sumanasekera, G. U.; Adu, C. K. W.; Fang, S.; Eklund, P. C. *Phys. Rev. Lett.* **2000**, *85*, 1096−1099.
(33) Jhi, S.-H.; Louie, S. G.; Cohen, M. L. *Phys. Rev. Lett* **2000**, *85*, 1710−1713.

(34) Mawhinney, D. B.; Naumenko, V.; Kuznetsova, A.; Yates, J. T., Jr.; Liu, J.; Smalley, R. E. *Chem. Phys. Lett.* **2000**, *324*, 213−216.
(35) Hu, H.; Bhowmik, P.; Zhao, B.; Hamon, M. A.; Itkis, M. E.; Haddon, R. C. *Chem. Phys. Lett.* **2001**, *345*, 25−28.
(36) Bahr, J. L.; Yang, J.; Kosynkin, D. V.; Bronikowski, M. J.; Smalley, R. E.; Tour, J. M. *J. Am. Chem. Soc.* **2001**, *123*, 6536−6542.
(37) Chen, J.; Rao, A. M.; Lyuksyutov, S.; Itkis, M. E.; Hamon, M. A.; Hu, H.; Cohn, R. W.; Eklund, P. W.; Colbert, D. T.; Smalley, R. E.; Haddon, R. C. *J. Phys. Chem. B* **2001**, *105*, 2525−2528.
(38) Kazaoui, S.; Minami, N.; Jacquemin, R.; Kataura, H.; Achiba, Y. *Phys. Rev. B* **2001**, *60*, 13339−13342.
(39) Bower, C.; Kleinhammes, A.; Wu, Y.; Zhou, O. *Chem. Phys. Lett.* **1998**, *288*, 481.
(40) Dresselhaus, M. S.; Dresselhaus, G. *Intercalation compounds of graphite*; Martin, D. H., Ed.; Taylor & Francis Ltd: London, 1981; Vol. 30, pp 139−326.

NL0156639